X-Ray Spectroscopy for Electrostatic Potential and Material Determination of Space Objects

Kieran Wilson and Hanspeter Schaub

***Abstract*— Measuring the charge on a nearby space object during close proximity, servicing, and rendezvous and docking operations without requiring physical touch remains challenging despite decades worth of data on spacecraft charging and its risks. This paper proposes the means to identify the charge on a closely neighboring space object and its elemental composition by examining the X-ray spectrum generated by energetic electrons impacting the target. In particular, deconvolution of the bremsstrahlung X-ray continuum provides an estimate of the landing energy of the electrons. Knowing the initial electron energy, the potential difference between the source and the target is determined. Additionally, characteristic X-rays emitted during the process of energetic electron–matter impact allows the relative abundance of elements in the target to be determined. Spatial separations in the order of tens of meters are required between an electron gun and the corresponding detector to maximize the collection of the bremsstrahlung spectrum. This could be achieved with either the single-craft and deployable booms or through the use of two spacecraft. Electron beam energies of 40 kV are found to generate sufficient levels of X-rays for potential determination at over 10 m from the target and to determine the landing energy of the beam to within 0.14% using commercial X-ray detectors.**

***Index Terms*— Space technology, voltage Measurement, X-ray detectors.**

I. Introduction

ELECTROSTATIC charging has been a known consequence of spaceflight since the early days of space exploration. As spacecraft interact with the space environment, they experience currents as a result of electron emission induced by the photoelectric effect of the sun's radiation and through currents of electrons and ions in the space plasma [1]. Several experiments have sought to characterize the charging environment at geostationary orbit (GEO); notably, SCATHA and ATS-6 missions that flew at GEOs in the 1980s demonstrated that spacecraft operating at GEO could charge to tens of kilovolts under certain conditions [2].

These missions also demonstrated the use of active charge control using electron or ion guns [3]. Whether natural or forced, spacecraft charging can create dangerous situations for spacecraft, as differential charging can result in arcing and potential electronics damage. Differentially charged spacecraft components can lead to arcing hazards, a frequent cause of damage to solar panels [4]. Brandhorst [5] found that half of the satellite insurance claims to be the result of solar panel anomalies, motivating a need to better understand charge distributions on spacecraft to mitigate such issues.

This threat also applies in rendezvous and servicing missions, as bodies charged to different potentials may experience damaging arcing as they contact [1]. In low earth orbit (LEO), Carruth and Ferguson [6] determine that under certain conditions, charge differentials could be significant enough to injure or kill astronauts performing extravehicular activities without proper mitigation.

However, thus far, it has only been possible to measure the potential on an instrumented craft itself. In many proposed missions to service, refuel, or reorbit spacecraft involving multiple bodies, knowing the charge of only one would be insufficient information to prevent arcing. Such methods also cannot provide needed information for the proposed missions that seek to harness the electrostatics for touchless object manipulation, such as the electrostatic tractor concept for remotely reorbiting debris away from the operating geostationary satellites or detumbling the space debris touchlessly [7], [8]. Other missions have been proposed to utilize Coulomb forces to establish spacecraft constellations, enabling missions, via fuelless formation flying, which are impossible to do with monolithic spacecraft and without plume impingement contamination and fuel consumption issues that come with traditional thrusters [9].

In addition to enabling a range of novel mission concepts, the ability to measure spacecraft potentials touchlessly *in situ* will contribute to the overall understanding of spacecraft charging and lead to better methods for mitigating potentially hazardous charging conditions.

Prior work on charge sensing has largely focused on measuring a spacecraft's own charge, as an indicator of potentially dangerous charge situations in which operators could take steps to mitigate. However, some methods have been proposed to measure the charge on a spacecraft or celestial object remotely [10]–[12].

Knowledge of the charge of one spacecraft at GEO is insufficient to determine the charge of even nearby objects, as demonstrated by Koons *et al.* [13] using data from seven geostationary spacecraft equipped with charge sensors. They found no relation between the charge states of spacecraft separated by just 0.4 h of local time (5.5° of longitude). Koons *et al.* [13] also determined that for the

Manuscript received October 5, 2018; revised March 4, 2019; accepted April 7, 2019. Date of publication May 7, 2019; date of current version August 9, 2019. The review of this paper was arranged by Senior Editor H. B. Garrett. *(Corresponding author: Kieran Wilson.)*

The authors are with the Ann and H.J. Smead Aerospace Engineering Sciences Department, University of Colorado at Boulder, Boulder, CO 80309 USA (e-mail: kieran.wilson@colorado.edu; hanspeter.schaub@colorado.edu).

Color versions of one or more of the figures in this paper are available online at http://ieeexplore.ieee.org.

Digital Object Identifier 10.1109/TPS.2019.2910576

awareness of hazardous charging conditions or anomaly diagnosis, the state of neighboring spacecraft was effectively irrelevant, further reinforcing the need for remote potential determination [13].

Several methods have been proposed to fill this gap and allow the remote determination of charge for spacecraft. Ferguson *et al.* [11] propose a series of techniques that could provide remote indications of charging or arcing events on spacecraft, utilizing the electromagnetic radiation, including surface glows, bremsstrahlung X-rays, and radio or optical emission from arcing, to provide a measure of charge buildup. Ferguson *et al.* conclude that detecting arcing events on GPS satellites may be possible from ground-based radio telescopes, but other optical methods would require nearby spacecraft to determine the occurrence of charging events. Additionally, the methods proposed cannot determine the level of charging occurring but can only indicate that it is happening.

Another approach provides an estimate of the voltage level based on secondary electrons generated in a material. Secondary electrons leave atoms with near-zero initial energy, so determining the energy they arrive at a collector, which allows the potential difference between the source and the collector to be determined. Halekas *et al.* [10] demonstrated this concept with data from the Lunar Prospector mission to determine the charge of the Moon's surface during solar energetic particle events. This method has also found success in measuring the surface potentials of targets in scanning electron microscopy (SEM), where it is widely used [14]–[16]. This method requires an electron detector positively biased relative to the surface being investigated to collect the ejected electrons.

Using the evolution of relative position and velocity measurements between two spacecraft over time due to the Coulomb force, Bennett [17] proposes a method for inferring the overall charge on a target craft. This method has limitations associated with temporal resolution (requiring minutes to hours to update the estimate of charge), charge resolution (which will be affected by the accuracy of gravitational models and models of relative motion), and spatial resolution (only the total charge can be determined as an effective sphere model).

An alternative method for close proximity charge determination is presented by Engwerda [12] and Engwerda *et al.* [18] who proposes to measure the electric field around an object and, from there, to estimate the voltage and generate a multisphere model of charge distribution on the object. This paper does not consider the difficulties associated with accurately measuring electric fields in an active charging scenario, nor in the sparse, hot plasma found at GEO. Furthermore, this preliminary study makes the strong assumption of planar relative motion with a known trajectory.

Another category of remote charge sensing involves analyzing the electromagnetic radiation released when energetic particles impact a charged object. For instance, Lamoureux [19] considers the means of determining the landing energy characteristics of an electron population based on observations of the resultant X-ray spectrum. They present deconvolution schemes for monoenergetic beams as well as different plasmas, providing a baseline mechanism for extracting landing energy from an X-ray spectrum [19]. This method has also been applied to measuring surface potentials of targets in electron microscopy with varying success. Belhaj *et al.* [14] find the method to be unreliable in a microsocopy context, where high-energy backscattered electrons impact surfaces near the target and generate contaminating X-ray spectra there. Others have found higher levels of success, and it is expected that in a space-flight-like environment, the macroscale geometry would mitigate the issues observed by Belhaj in micro-scale analysis [20], [21].

This X-ray spectrum also contains peaks that can be used to determine the elemental composition of a material. This has been applied in spaceflight previously and is used by the REXIS instrument aboard Osiris-Rex to map the elemental distribution across the surface of the asteroid Bennu. Instead of using energetic electrons to generate X-rays, REXIS relies on the characteristic X-ray fluorescence caused by the solar X-ray excitation of the asteroid's surface [22].

This paper studies the use of an electron gun on the primary spacecraft targeting the electron emission onto the neighboring space object. The resulting X-rays provide a method to measure both local potential and material properties. The challenge is to determine what beam energies are required to create a strong enough return, how to measure the return signal, and to what accuracy the charge could be sensed. The novelty of this paper is that it allows for charge sensing on a neighboring spacecraft or space object without physical touch. Furthermore, in contrast to measuring secondary electron emission or inferring charge level from the perturbed relative motion, the X-ray-based technique is able to perform high spatial resolution component charge and material property measurements within the space object structure.

This paper is organized as follows. First, the bremsstrahlung-based charge sensing method is discussed as well as the physics and challenges associated with the characteristic radiation and the bremsstrahlung effect itself. Next, the numerical modeling of bremsstrahlung is described, which allows for a numerical study of the electron landing energies and the resulting characteristic radiation. Implementation challenges, such as sensor considerations, power, and mass, are discussed to evaluate the feasibility of this concept.

II. Sensing Method Overview

The method of material composition and potential determination studied in this paper is reliant on the use of an electron beam to generate X-rays at the target. Many complex phenomena occur when an electron beam impacts the material surface, as shown in Fig. 1. Bremsstrahlung X-ray generation is related to the landing energy of the electrons when they reach the material, which is a function of the voltage of the material and the energy of the electron beam. By measuring the X-ray emission and knowing the energy of the electron beam, the voltage of the material can be determined. The X-rays emitted by the electron state changes, known as the characteristic X-rays, are another product of this interaction and can additionally be used to determine the elemental composition of the target. An implementation of this concept

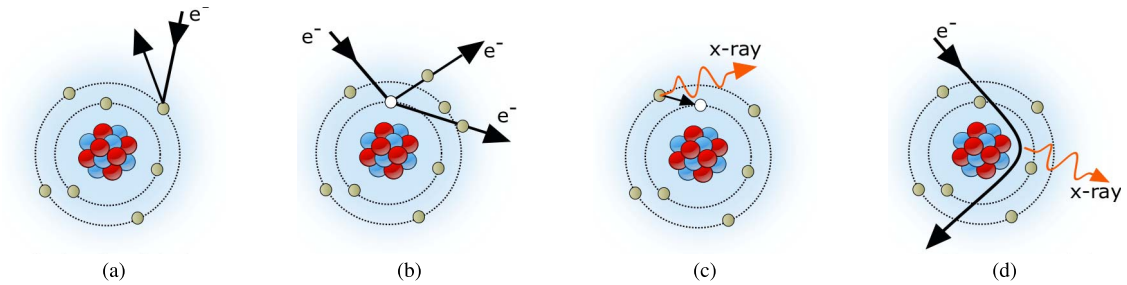

Fig. 1. Four dominant interactions between energetic electrons and matter. (a) Backscattered electron. (b) Incoming electron knocking a secondary electron free of the atom. (c) Outer orbital electron dropping to fill the vacancy left by the secondary and releasing characteristic X-ray radiation. (d) Electron deflected by the positive charge of the nucleus and emitting a bremsstrahlung X-ray.

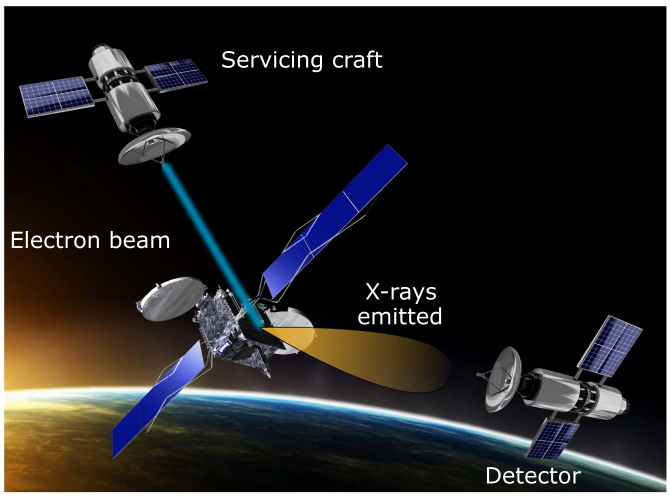

Fig. 2. Concept of operations for a two-craft sensing configuration, where one uses an electron beam to generate X-rays that are collected by a second craft.

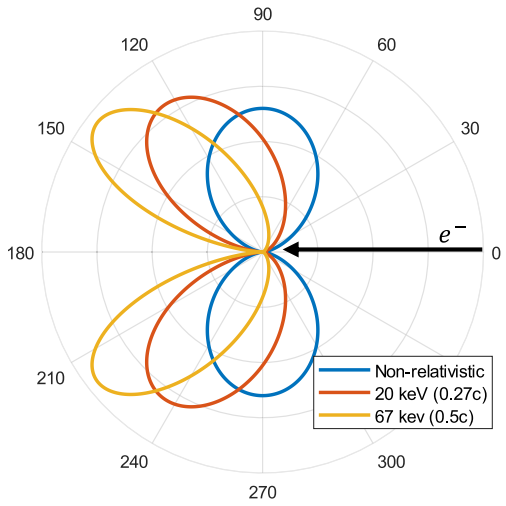

Fig. 3. Angles of bremsstrahlung emission as a function of the incident electron energy. The electron follows the black arrow and interacts with an atom at the origin.

to determine the surface charge and material composition of a defunct spacecraft is shown in Fig. 2. Because the majority of the generated X-rays from relativistic electrons are emitted in the direction of the beam, a second spacecraft or long boom may be needed to place the X-ray detector, where it can get the strongest signal.

III. Bremsstrahlung Description

As the electrons approach a material, they are subject to accelerations as a result of the voltage of the material either attracting or repelling the electrons. When the electrons collide with the atoms in the material, they slow down and release energy as photons. Because the electrons will slow down by different amounts depending on their exact trajectory in the vicinity of the atomic nucleus, this results in a continuous energy spectrum. This continuous energy spectrum is observed predominantly in X-ray energies and is known as bremsstrahlung (German for "braking radiation") [23].

The highest energy photons that can be released by this process result from the case, where an incoming electron is completely stopped by an atom, releasing its full kinetic energy as a single X-ray. The wavelength of such a photon is given by the Duane–Hunt law, as

$$\lambda_{\min} = \frac{hc}{eV} \tag{1}$$

where h is the Plank's constant, c is the speed of light, e is the electron charge, and V is the accelerating potential [24].

Therefore, an upper limit for photon energy exists, equal to the energy of the incident electron; electrons with a landing energy of 40 keV will generate a bremsstrahlung spectrum with a maximum energy cutoff of 40 keV.

A. Angular Distributions

When electrons curve around atoms and lose energy, they emit photons in the direction normal to the acceleration, as shown in Fig. 1(d). The angle of emission of the resultant bremsstrahlung continuum radiation is dependent on the energy of the incident electron; to a first-order approximation, the power radiated as a function of angle can be related to incident electron beam energy by

$$P(\theta) \propto \frac{\sin^2(\theta)}{(1-\beta\cos(\theta))^5} \tag{2}$$

where θ is the angle relative to the electron beam and $\beta = (v_{\text{electron}}/c)$ with c taken as the speed of light [26]. This relation is illustrated in Fig. 3 for three incident electron energies.

While this is a fairly simplistic approximation, it serves primarily to understand the underlying trends. As shown

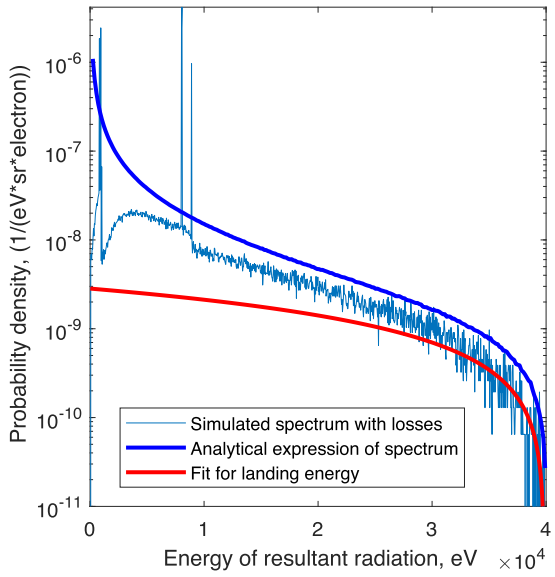

Fig. 4. Resultant X-ray spectrum illustrating both the bremsstrahlung continuum and the sharp peaks of the characteristic X-ray emission, analytic curve from [25].

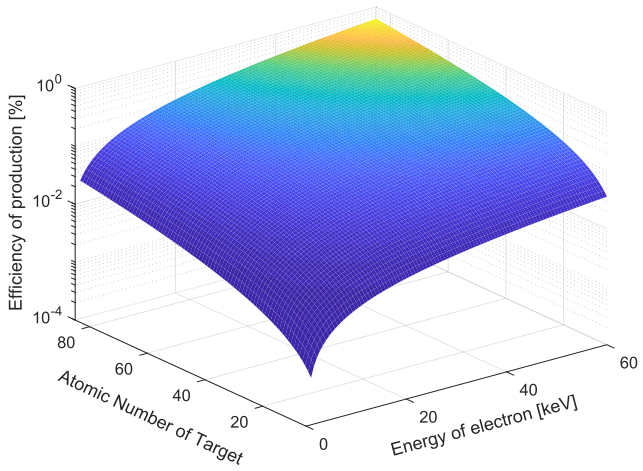

Fig. 5. Radiation yield as a function of atomic number of the target and incident energy of the electron. The maximum yield here is 0.64%.

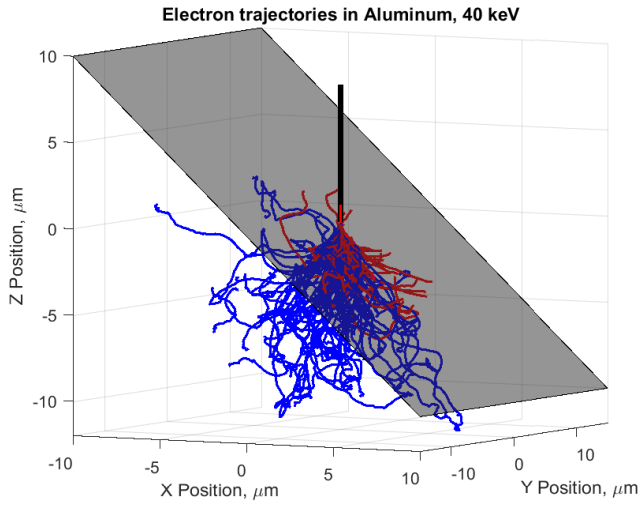

Fig. 6. 40-keV electron trajectories through an aluminum target, generated in pyPenelope. Red trajectories indicate electrons that are backscattered, and blue paths indicate those that were absorbed. The material boundary is indicated by the gray surface, and the black line is the incident electron beam originating in the +Z-direction.

in Fig. 4, increasing the energy of the electron beam results in increasingly forward-directed photons. At nonrelativistic velocities, the primary radiation direction is nearly orthogonal to the incident beam; however, for 20-keV electrons, the peak angle of radiation emission is 125° from the incident electron beam. This trend continues for higher energies with MeV-level electrons emitting photons in nearly the same direction as the incident electrons traveling. Increasing the landing energy has the effect of increasing the total energy radiated in proportion to E_0^2, while the output becomes more highly directed, effects that combine to improve numbers of photons detected at the optimal position.

The bremsstrahlung spectrum is doubly differential in angle and in energy. As the angle of the observer relative to the incident electron beam varies, the observed energy spectrum will vary as well.

B. Radiation Yield

Yield is described as an efficiency term, comparing energy deposited by the electrons to energy radiated by photons. One description developed by Kulenkopff proposes the efficiency to be a function of energy and atomic number of the target material of the form

$$\varepsilon = a(ZV_0 + 16.3Z^2) \tag{3}$$

where a is an empirically derived constant (found to be 1.2×10^{-9}) and V_0 is the electron energy in eV [26]. The efficiency, therefore, increases proportionately to V_0 and as the square of Z. For high Z materials, the Z^2 term becomes important, while for low Z materials, the first term remains dominant. For 40-keV electrons interacting with aluminum ($Z = 13$), the efficiency is $\varepsilon = 0.06\%$, while the same electrons hitting gold ($Z = 79$) would have an efficiency of $\varepsilon = 0.39\%$. This relation can be seen in Fig. 5.

The fraction of incident beam energy that is emitted as bremsstrahlung radiation is proportional to the incident beam energy and to the square of the atomic number of the material Z [23]. Average yields for typical spacecraft materials, such as aluminum ($Z = 13$) or Kapton ($Z_{\text{eff}} \approx 8.4$), are assumed to be in the order of 0.01%–0.1% for the energies under consideration here (up to 50 keV), increasing closer to 1% for high atomic mass elements, such as gold.

X-rays generated near the surface of a sample have a greater likelihood of escaping, rather than being absorbed by another atom [27]. Additionally, the forward-directional nature of energetic bremsstrahlung radiation seen in Fig. 3 means that a highly inclined target, where a greater fraction of the interactions take place near the surface and there is less material in the direction of the bremsstrahlung emission lobe, is favorable for the X-ray detection. Fig. 6 illustrates the path of an electron shower in an inclined aluminum

thick target. At each interaction, the electrons lose energy either through the ionization of the impacted atom or through the bremsstrahlung radiation. Target self-absorption of the generated X-rays is less significant for a surface that is highly inclined relative to the incident electron beam than for the one that is near perpendicular due to the forward-directional bias of bremsstrahlung [23]. Therefore, a higher fraction of generated X-rays will escape the target when the electron beam is at a grazing incidence than when it is normal to a surface, improving the detection probabilities.

The interaction shown in Fig. 1(a) results in electrons being reflected back out of a target, rather than depositing their full energy in the material. Around 10% of electrons in the energy range of interest experience backscattering, which involves accelerating electrons in manners that also generate bremsstrahlung X-rays. These X-rays form additional lobes closer to the direction of the incident electron beam than the lobes shown in Fig. 3 and could potentially negate the need for extended booms or multiple spacecraft to observe the emitted X-rays [28]. This is an area of further research.

IV. Modeling of X-Ray Emission

A wide range of factors affect the X-ray spectrum at a given point, including the incident electron beam energy, the angle between the beam and the detector, and the target material. To gain insight into this process, several of these aspects are analyzed using fairly simple approximations, and the final results are confirmed using the sophisticated Monte Carlo-based modeling codes.

Bremsstrahlung can be subdivided by various categories that affect the methods available to analyze and simulate it. One of the most significant describes the nature of the target, as either a thin or thick sample. "Thin" refers to a specimen, in which an incident electron is likely to have only one interaction with an atom before being transmitted; in this case, there is a little absorption of the generated radiation by the sample, and the electrons all have the same initial energy prior to their interaction. The So-called thick targets, meanwhile, have a large fraction of the incident electrons absorbed by the target after a series of energy-shedding interactions and are the subject of analysis here. Because the electrons interact with a large number of atoms as they lose energy, the resultant bremsstrahlung spectrum is distinctly different from that generated by the thin-target interactions [19]. Additionally, the surrounding atoms absorb some of the bremsstrahlung X-rays before they can be emitted outside of the target; low-energy photons are particularly susceptible to absorption, depressing the number of photons emitted in higher wavelength parts of the spectrum, as shown in Fig. 4 [26], [27].

Bremsstrahlung can arise as a result of an energetic electron accelerating in the vicinity of an atom or by undergoing polarization in an electron cloud. Polarizational bremsstrahlung is a fairly small effect relative to atomic for the problem under consideration here, so the focus in this paper will be on atomic or classical bremsstrahlung [26].

Incident electron energies of interest are likely to be in the region of 10–60 keV, based on an anticipated beam energy of 30–40 kV and a potential difference to the target of up to 20 kV. This range is in the realm of mildly relativistic electrons, where relativistic effects cannot be ignored but neither are high-energy approximations appropriate [a 10-keV electron has $\beta = (v/c) = 0.195$, while 60 keV is $\beta = 0.446$]. Therefore, the problem of interest can be narrowed to the generation of X-rays in a thick target by mildly relativistic electrons, a problem that is well described by the Koch and Motz 2BN model discussed earlier [29]. In addition to the analytic implementation described earlier, this model is integrated into the pyPENELOPE Monte Carlo framework for simulating the electron–matter interaction. Simulation of the bremsstrahlung spectrum was performed mainly in pyPenelepe, an open-source Python-based framework for the widely used PENELOPE Monte Carlo codes. Penelope makes use of a variety of methods for simulating the coupled electron–photon transport and formation [30]. This code was used to generate the simulated bremsstrahlung spectra shown in Fig. 4 as well as the electron trajectories in Fig. 6.

A. Spectral Distribution

The bremsstrahlung spectrum has maximum cutoff energy, discussed earlier in (1). Additionally, due to the self-absorption of longer wavelengths by surrounding atoms, the emitted flux is expected to decay to zero, as the energy approaches zero, as shown in Fig. 4.

Empirical models exist to describe the thick-target bremsstrahlung distribution, such as that of Kulenkampff, which is insensitive to how relativistic the incident electrons are [26]. This model is used to generate the spectra at three energies in Fig. 3.

A basic model of the energy spectrum is provided by the Kramer's Law, which can be written as

$$I(\lambda)d\lambda = \frac{K}{\lambda^2}\left(\frac{\lambda}{\lambda_{\max}} - 1\right) \tag{4}$$

where K is a constant that varies proportionally with the atomic number of the target element [26].

This model is a reasonable starting approximation but fails to account for absorption of the X-rays by the target material or electron backscattering, effects that can be quite significant for thick targets. Analytic modifications have been proposed to improve the accuracy of the model for thick targets, most notably by Brunetto and Riveros [25]. The Koch and Motz 2BN model is accurate to within 10% for the energy range under consideration here and is the most accurate analytic model available for the mildly relativistic thick-target bremsstrahlung [29]. This model provides the analytic curve (in blue) shown along with a simulation of the detected spectrum in Fig. 4.

B. Landing Energy Determination

The simplest approach to determining the electron landing energy would be to determine the maximum X-ray energy detected. As discussed earlier, this maximum X-ray energy is equivalent to the case where the electron is fully stopped and its full landing energy is converted to an X-ray with energy in the limit of the Duane–Hunt law in (1).

However, several issues are raised by this method. First, the sun emits significant quantities of hard X-rays, so any small quantity of high-energy X-rays could be the product of bremsstrahlung at the site by the electron beam or of solar emissions or even the result of high-energy electrons in the ambient plasma creating bremsstrahlung interactions. Additionally, the number of electrons that are fully stopped in one collision is vanishingly small, and the chance of detecting such an X-ray in a realistic scenario with a small detector far from the origin is smaller still. Therefore, very long collection times would be required to have a significant sample near the very limit of the energy range and would require no solar X-ray interference and sophisticated filtering of sensor noise. This approach is widely applied to determining the potential of a target object in SEM [20], [21].

Alternatively, Lameroux [19] propose a more robust method for determining the landing energy of the electrons via deconvolution of the bremsstrahlung spectrum. For a spectrum resulting from a monoenergetic incident electron beam, a linear fit to the high-energy portion of the spectrum (where $E > 0.9E_0$) is recommended. This line has the landing energy of the electron beam as its x-intercept, allowing a straightforward means of determining the landing energy, as shown by the red line in Fig. 4.

V. Characteristic Radiation

The bremsstrahlung continuum provides a means of identifying the electrostatic potential of a surface. However, the characteristic radiation emitted through the electron–matter interaction can provide another important assessment of a surface: the elemental composition.

In addition to the bremsstrahlung continuum radiation, characteristic radiation is emitted as a byproduct of ionization interactions in the target material. When the incident electron excites an inner-shell electron in the target material causing its ejection, the resulting vacancy is filled by an outer shell electron. This electron releases a photon as it relaxes to an empty energy state with energy equal to the difference in energy of the two shells. Because this energy difference is specific to the atom, the radiation can be used to identify the element. The energy difference between the two shells is emitted as a photon, the energy of which can be used to determine the electron transition and element it originated from. While these photons are emitted isotropically, spectroscopy for elemental identification of the target is easier in areas away from the primary bremsstrahlung lobe to avoid masking the characteristic radiation signal, as shown in Fig. 7.

The characteristic spikes can be observed in Figs. 4 and 7 as the sharp peaks in the simulated X-ray spectrum. Each peak corresponds to an electronic transition, as a valence (outer level) electron falls to a lower energy state to fill a vacancy formed when an inner electron is ejected by an impacting electron.

These peaks allow the material to be identified as copper in Fig. 4, while Fig. 7 shows the spectrum resulting from Al2195, an aluminum–lithium alloy commonly used in spacecraft and rocket bodies [31]. From this spectrum, it is relatively straightforward to identify aluminum as the dominant element, based on the relative level of the peaks; the relative concentrations of the alloying elements (lithium, copper, silver, and magnesium) can be determined by a similar process.

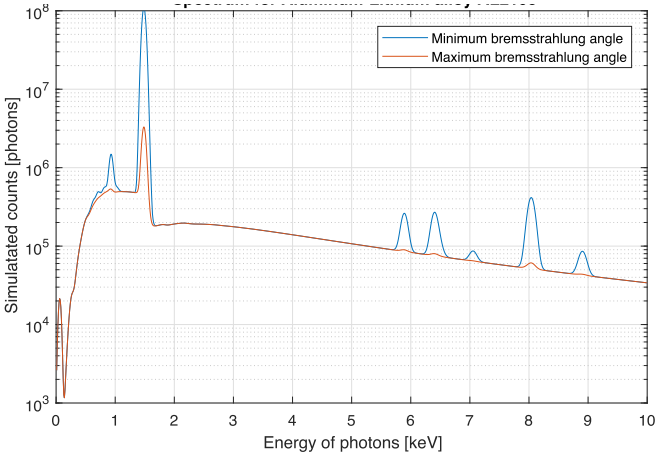

Fig. 7. Near maximum and minimum bremsstrahlung spectra, normalized by the magnitude of the spectrum to allow for comparison between the relative magnitude of the characteristic spike and the continuum spectrum.

An open-source program developed by National Institute of Standards and Technology (NIST) for energy dispersive X-ray spectroscopy, DTSA-II, was used to simulate and analyze the characteristic spectra generated and was used to generate the curves in Fig. 7 [32]. It is worth noting that while the complete set of peaks is unique to a specific element, some transitions can be very similar between elements, complicating identification [23], [32].

While the characteristic peaks provide a useful means of determining a surface's composition, many spacecraft make use of aluminized Mylar or Kapton for thermal control, often as a part of multilayer insulation (MLI). While coated in a metal, MLI is primarily composed of dielectric materials, which could lead to false conclusions about the charge capacity and conductivity of sections of the craft. However, as shown in Fig. 6, 40-keV electrons penetrate over 10 μm into a material (the NIST ESTAR database gives the range of 40-keV electrons into aluminum as 15 μm) [33]. For comparison, typical metallic coatings used for thermoregulation of spacecraft are on the order of 0.1 μm in thickness [34]. Therefore, even if a surface is covered in a layer of gold or aluminum, the substrate material can still be identified via the characteristic radiation generated by the penetrating electrons.

VI. Implementation

When considering how the system discussed could be implemented in the real world, several significant factors must be addressed. Defunct spacecraft in GEO frequently have high rotational rates, up to tens of degrees per second [35]. Because of the risk of a collision, separation distances between the target and the servicing craft of at least the radius of the craft are desired, taken here to be in the order of 10 m. Additionally, sensors must be selected with sufficient resolution and detector area to provide an accurate assessment of material composition and surface potential. Finally, the components of the system must be capable of performing in the space environment.

A. Boom Versus Two Craft

First, the forward-directional nature of bremsstrahlung poses spatial constraints due to the separation required between the detector and the electron source. As discussed earlier and illustrated in Fig. 3, bremsstrahlung emission's peak emission direction is a function primarily of incident electron energy. For an electron beam with a 10-keV landing energy, the direction of peak emission is 115.6° from the direction of the beam source; for a 60-keV beam, the angle will be 142°.

Assuming a standoff distance of 10 m, even a 10-keV beam (which has a relatively small X-ray emission angle) would require over 20 m of linear separation between the beam source and the X-ray detector, a challenging distance to achieve with one craft. Furthermore, 10 m is likely to be at the lower end of acceptable distances to tumbling multiton spacecraft, necessitating further distances with larger separations. Likewise, the increasing separation distance required by increasing landing energies and changing the direction of peak emission suggests that this would be best approached as a formation flying problem with separate craft carrying the electron gun and the X-ray detector. This solution would also enable new approaches to prior proposed electrostatic actuation of uncontrolled craft, potentially allowing improvements in performance over detumbling and reorbiting scenarios that have been previously explored [17].

However, a boom-based solution utilizing only one craft may still be functional for certain missions, and the limitations of this approach are the subject of future work. No requirements are placed on the location of the sensor relative to the detector for characteristic radiation detection. Additionally, the backscattering discussed earlier could improve the viability of this method by reducing the separation required. Booms have previously been developed and flow with lengths of over 100 m though these systems have a fixed deployed length [36]. Such a design could potentially be adapted to support an X-ray spectrometer for sensing applications.

B. Sensor Considerations

Any optical sensor is subject to noise and limits to the size of the detector with larger detectors capable of receiving more photons and typically reduced levels of noise.

Furthermore, X-ray detectors have efficiency curves as a function of energy, performing much better at some wavelengths than others. At low energies, this attenuation is typically the result of absorption by the detector window, while high energies typically interact less strongly with the sensor and may instead pass through and interact with the material behind the sensor [37].

Because only 0.1% of the photons generated are in the range of $E > 0.9E_0$ and just 0.08% of electron kinetic energy is converted to photons, even a relatively large X-ray sensor of 70 mm^2 at 10 m to the target will be hit by an energy flux of just 5×10^{-10} times the incident power of the electron beam. However, this still translates to a total of 3.5×10^6 photons/s in this high-energy range based on an assumed electron gun with a current of 1 mA and emission potential of 40 kV for a total power output of 40 W.

For this application, commercial versions of two sensor types (either higher resolution silicon drift detectors or lower resolution but larger Si-PIN detectors) could be implemented with tradeoffs between sensor resolution, related to the accuracy of landing energy measurement, and size, which affects the number of photons collected and, therefore, temporal resolution [38]. Temporal resolution is important as the electron gun operation will alter the charge of the target craft over time, so minimizing the collection time can reduce the resultant perturbation of the object's charge. Additionally, for a tumbling target, the improved temporal resolution will result in a higher fidelity model of the target's elemental composition and a better understanding of the charge distribution on the target.

Available off-the-shelf commercial sensors have energy resolutions of around 120 eV and active detector areas of up to 70 mm^2 (based on the Amptek Fast SDD that has flight heritage on the Neutron star Interior Composition Explorer, or NICER, mission) [38], [39]. Using this sensor as a baseline with a 40-keV electron beam, 10-m standoff distance, and 1-mA current, a usable signal would take on the order of a millisecond to collect if the detectors were at the optimal position. This time could be reduced further through the use of grazing incidence X-ray optics, such as those developed for use by NSICER's X-ray detectors. The efficiency of these optics decays rapidly as energy increases, falling from nearly 40% at 1.5 keV to less than 5% at 10 keV [40]. Nonetheless, the use of such optics can provide a means of effectively amplifying low-energy X-ray signals, decreasing collection time accordingly. For the NICER mission, 10-cm^2 concentrating optics were used with an effective surface area of 44 cm^2 at 1.5 keV or 18 cm^2 at 4.5 keV after accounting for losses [40]. Even with the smaller effective area, this represents over a 25-fold increase over the use of the detector alone and would correspondingly decrease the collection time to less than 10^{-4} s. X-ray concentrators optimized for higher energy photons have also been designed for spaceflight [41].

At such short collection times, detector dynamics become important limitations. High rate detectors, such as the Amptek Fast SDD, saturates at count rates greater than 1 million photons/s, while other available detectors have maximum count rates on the order of 100 000 per second or lower [38]. However, because the landing energy deconvolution method used is reliant only on the high-energy portion of the bremsstrahlung spectrum, this limitation can be mitigated through careful selection of shielding materials to act as a window for the detector, which prevents saturation by blocking lower energy X-rays.

While temporal resolutions of milliseconds are achievable, it is important to consider the rate of charging of the target object during these measurements. For the case utilizing an electron beam, [42] provides an overview of charging dynamics and limitations at GEO for both the target and the servicing craft. For a rough approximation of the charging during measurement with an active electron beam, the target is assumed to be a sphere with a relationship between surface potential ϕ and charge Q controlled only by the charge

added as

$$\Delta\phi = (1-\delta)\frac{\Delta Q_{\text{beam}}}{4\pi\varepsilon_0 r}. \tag{5}$$

For a 10-m-diameter aluminum sphere illuminated by a 40-keV electron beam and a secondary electron yield of $\delta = 0.3$, the surface potential will change by around 500 V during measurement. This calculation is only approximate, as it neglects photoelectric currents, those from the ambient plasma ions and electrons and other current sources, which are likely to reduce the overall potential change. For the case of the electrostatic tractor, where such a beam is used continuously and the target and servicer are maintained in electrostatic equilibrium, the change in potential is canceled out by ambient currents, so this will lead to an accurate steady-state reading. However, this could problematically perturb the potential of naturally charged objects. One solution would be to reduce the beam current, to allow ambient currents to mitigate the charging effect, and using a longer data collection interval. Knowing the effect of the electron beam on the servicing craft's potential could allow the potential induced by the beam to be subtracted from the measured target potential to find its steady-state charge level.

Additionally, it may be possible to use ambient energetic electrons found in the magnetosphere to generate a measurable quantity of bremsstrahlung X-rays that could be used to determine the potential of the target relative to the plasma environment. This is an area of future work on this subject.

To analyze the dependence of the bremsstrahlung spectrum on angle and energy, the Koch and Motz 2BN model, an analytic expression optimized for low-energy (mildly relativistic) electrons, was implemented in MATLAB [29]. This expression provides the shape and the intensity of the spectrum at any angle to the incident electron beam.

Because of the deconvolution scheme used to determine the landing energy of the electrons is based on the trend of the high-energy X-ray data, the accuracy of the landing energy calculation is only somewhat related to the accuracy of the computed landing energy. This relationship is illustrated in Fig. 8. Despite a simulated detector resolution of 490 eV, this method was still able to determine the landing energy of the electrons in the worst case sensor in Fig. 8 to within 54 eV, less than 0.14% of total error.

Reducing the resolution of the sensor, however, will have a negative impact on resolving characteristic lines and, therefore, on the ability to determine material composition. Additionally, care must be taken to exclude the solar radiation from the sensor, as trace amounts of heavy elements in the corona are energized to emit characteristic X-rays that could make determination of the target material more difficult [43]. Careful selection of detector window materials and baffles or Soller slits along with minimizing sun-facing orientations should mitigate these concerns.

C. Power and Mass

The addition of any system to a spacecraft is critically evaluated for the impact of two scarce resources: power and mass. The booms described previously as a potential method for the single-craft operation have masses of less than 12 kg for a 100-m fixed-length boom with no direct power impact after deployment [36]. A two-craft system naturally has a higher power and mass impact than a system that can be integrated into only one spacecraft.

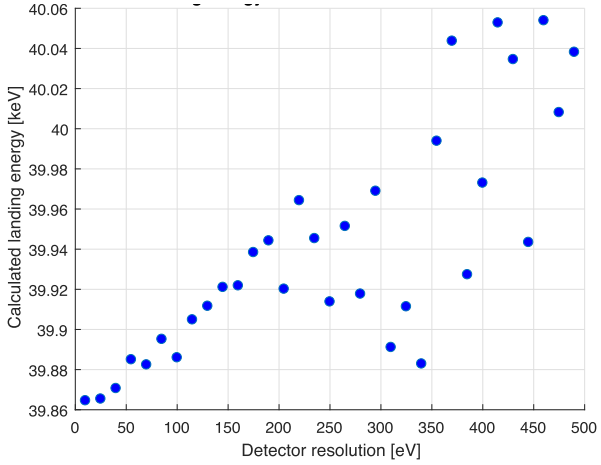

Fig. 8. Calculated landing energy as a function of detector resolution.

However, two crafts may provide performance benefits in many servicing or electrostatic reorbiting applications, mitigating the overall mission impact.

X-ray detectors with flight heritage in the NEAR and Mars Pathfinder missions consume less than 1 W and have a mass of less than 140 g (based on the Amptek detector analyzed for temporal resolution) [38]. This would have a limited impact on most spacecraft missions.

High-energy electron beams have been flown in space on prior missions. Notably, the EXOS-B and SCATHA satellites were equipped with electron guns up to 200-eV and 1-mA currents in the near-GEO space. In suborbital sounding rocket experiments, far more powerful electron guns have been tested in space. The ECHO-2 experiment carried pulsed beam electron gun with 80-mA current and 45-keV voltage on a similar scale to those proposed for use here [44].

Even higher energy systems have been studied for use in space; Neubert [45] proposes flying a linear accelerator emitting electrons with energies up to 5 MeV, declaring the technology feasible for orbital applications.

VII. Conclusion

A system is proposed to determine the electrostatic potential and elemental composition of a space object from distances of greater than 10 m. By using an electron gun with an energy of 40 kV and 1 mA, combined with an X-ray detector with a resolution of at least 400 eV, the landing energy of the electrons can be determined to sub-1% accuracy. All major elements of the system have some degree-of-flight heritage, improving the feasibility of this method. Additionally, this could enable future missions based on the electrostatic actuation of debris or rendezvous and servicing, opening up new opportunities for utilizing the space environment.

Low-earth orbital environments, specifically high densities of cold plasma, may make this method more difficult to implement due to uncertainty in the interaction of the electron

beam with the ambient plasmas. This is an area for future study. Additional work is required to determine the impact of a two-craft formation compared to the results that could be achieved by a single craft with a boom-mounted detector, particularly when accounting for the effects of backscattered electrons. The effect of a charged body on the trajectory of the electron beam should be considered more carefully as well.

REFERENCES

[1] S. T. Lai, *Fundamentals Spacecraft Charging: Spacecraft Interactions with Space Plasmas*. Cambridge, U.K.: Cambridge Univ. Press, 2011.

[2] E. G. Mullen, M. S. Gussenhoven, D. A. Hardy, T. A. Aggson, and B. G. Ledley, "SCATHA survey of high-voltage spacecraft charging in sunlight," *J. Geophys. Res.*, vol. 91, no. A2, pp. 1474–1490, 1986.

[3] R. C. Olsen, " Experiments in charge control at geosynchronous orbit-ATS-5 and ATS-6," *J. Spacecraft Rockets*, vol. 22, no. 3, pp. 254–264, May 1985.

[4] I. Katz, A. Davis, and D. Snyder, "Mechanism for spacecraft charging initiated destruction of solar arrays in GEO," in *Proc. AIAA Aerosp. Sci. Meeting Exhibit,* p. 1002, Jan. 1998.

[5] H. Brandhorst and J. Rodiek, "Improving space utilization by increasing solar array reliability," in *Proc. AAAI*, 2007, p. 6024.

[6] M. R. Carruth, Jr., *et al.*, "ISS and space environment interactions in event of plasma contactor failure," in *Proc. 7th Int. Conf. Spacecraft Charging Technol.*, R. A. Harris, Ed. Noordwijk, The Netherlands: ESTEC, Apr. 2001, p. 95.

[7] T. Bennett and H. Schaub, "Touchless electrostatic three-dimensional detumbling of large Axi-symmetric debris," *J. Astron. Sci.*, vol. 62, no. 3, pp. 233–253, Sep. 2015.

[8] E. Hogan and H. Schaub, "Relative motion control for two-spacecraft electrostatic orbit corrections," *AIAA J. Guid., Control, Dyn.*, vol. 36, no. 1, pp. 240–249, Nov. 2013.

[9] L. B. King, G. G. Parker, S. Deshmukh, and J.-H. Chong, "Spacecraft formation-flying using inter-vehicle coulomb forces," NASA/NIAC, Washington, DC, USA, Tech. Rep., Jan. 2002. [Online]. Available: http://www.niac.usra.edu/files/studies/final_report/601King.pdf

[10] J. Halekas *et al.*, "Extreme lunar surface charging during solar energetic particle events," *Geophys. Res. Lett.*, vol. 34, no. 2, Jan. 2007. doi: 10.1029/2006GL028517.

[11] D. C. Ferguson, J. Murray-Krezan, D. A. Barton, J. R. Dennison, and S. A. Gregory, "Feasibility of detecting spacecraft charging and arcing by remote sensing," *J. Spacecraft Rockets*, vol. 51, no. 6, pp. 1907–1913, Oct. 2014.

[12] H. Engwerda, "Remote sensing for spatial electrostatic characterization using the multi-sphere method," M.S. thesis, Dept. Aerosp. Eng., Delft Univ. Technol., Delft, The Netherlands, Mar. 2017.

[13] H. Koons, J. Mazur, A. Lopatin, D. Pitchford, A. Bogorad, and R. Herschitz, "Spatial and temporal correlation of spacecraft surface charging in geosynchronous orbit," *J. Spacecraft Rockets*, vol. 43, no. 1, pp. 178–185, Jan. 2006.

[14] M. Belhaj, O. Jbara, M. N. Filippov, E. I. Rau, and M. V. Andrianov, "Analysis of two methods of measurement of surface potential of insulators in SEM: Electron spectroscopy and X-ray spectroscopy methods," *Appl. Surf. Sci.*, vol. 177, nos. 1–2, pp. 58–65, Jun. 2001. [Online]. Available: http://www.sciencedirect.com/science/article/pii/S0169433201002094

[15] J. T. Heath, C.-S. Jiang, and M. M. Al-Jassim, "Measurement of semiconductor surface potential using the scanning electron microscope," *J. Appl. Phys.*, vol. 111, no. 4, Jan. 2012, Art. no. 046103.

[16] J. Cazaux, "Surface potential and SE detection in the SEM," in *Proc. EMC 14th Eur. Microscopy Congr.*, M. Luysberg, K. Tillmann, and T. Weirich, Eds. Berlin, Germany: Springer, 2008, pp. 519–520.

[17] T. J. Bennett, "On-orbit 3-dimensional electrostatic detumble for generic spacecraft geometries," Ph.D. dissertation, Dept. Aerosp. Eng. Sci., Univ. Colorado Boulder, Boulder, CO, USA, 2017.

[18] H. J. A. Engwerda, J. Hughes, and H. Schaub, "Remote sensing for planar electrostatic characterization using the multi-sphere method," in *Proc. Final Stardust Conf.*, Oct. 2016.

[19] M. Lamoureux and P. Charles, "General deconvolution of thin-target and thick-target Bremsstrahlung spectra to determine electron energy distributions," *Radiat. Phys. Chem.*, vol. 75, no. 10, pp. 1220–1231, Oct. 2006.

[20] M. Brochu, H. Demers, R. Gauvin, M. Pugh, and R. Drew, "Determination of e2 for nitride ceramics using fe-sem and the duane-hunt limit procedure," *Microscopy Microanalysis*, vol. 11, no. 1, pp. 56–65, Feb. 2005. [Online]. Available: https://colorado.idm.oclc.org/login?url=https://search-proquest-com.col% orado.idm.oclc.org/docview/220293454?accountid=14503

[21] D. C. Joy and C. S. Joy, "Low voltage scanning electron microscopy," *Micron*, vol. 27, nos. 3–4, pp. 247–263, Jun./Aug. 1996. [Online]. Available: http://www.sciencedirect.com/science/article/pii/0968432896000236

[22] R. A. Masterson *et al.*, "Regolith X-Ray imaging spectrometer (REXIS) aboard the OSIRIS-REx asteroid sample return mission," *Space Sci. Rev.*, vol. 214, no. 1, p. 48, Feb. 2018.

[23] G. Pavlinsky, *Fundamentals of X-Ray Physics*. Cambridge, U.K.: Cambridge Univ. Press, 2007.

[24] W. Duane and F. L. Hunt, "On X-ray wave-lengths," *Phys. Rev.*, vol. 6, no. 2, pp. 166–172, Aug. 1915. doi: 10.1103/PhysRev.6.166.

[25] M. G. Brunetto and J. A. Riveros, "A modification of Kramers' law for the X-ray continuum from thick targets," *X-Ray Spectrometry*, vol. 13, no. 2, pp. 60–63, Feb. 1984.

[26] A. A. M. Rene and E. Van Grieken, Ed., *Handbook X-Ray Spectrometry*, 2nd ed. New York, NY, USA: Marcel Dekker, Inc., 2002.

[27] S. Morelhao, *Computer Simulation Tools for X-Ray Analysis: Scattering and Diffraction Methods*. New York, NY, USA: Springer, 2016.

[28] L. Reimer, *Scanning Electron Microscopy: Physics of Image Formation and Microanalysis*, 2nd ed. New York, NY, USA: Springer, 1998.

[29] H. W. Koch and J. W. Motz, "Bremsstrahlung cross-section formulas and related data," *Rev. Mod. Phys.*, vol. 31, no. 4, p. 920, Oct. 1959.

[30] F. Salvat, J. M. Fernández-Varea, and J. Sempau, "Penelope 2006: A code system for Monte Carlo simulation of electron and photon transport," Organisation Econ. Cooperation Develop. (OECD), Paris, France, Tech. Rep. NEA No. 6222, 2006.

[31] "Super lightweight external tank," NASA, Washington, DC, USA, Tech. Rep. FS-2003-06-70-MSFC, 2005.

[32] N. W. Ritchie, "Efficient simulation of secondary fluorescence via NIST DTSA-II Monte Carlo," *Microsc. Microanal.*, vol. 23, no. 3, pp. 618–633, Jun. 2017.

[33] M. J. Berger, J. Coursey, M. Zucker, and J. Chang, *ESTAR, PSTAR, and ASTAR: Computer Programs for Calculating Stopping-Power and Range Tables for Electrons, Protons, and Helium Ions*. Gaithersburg, MD, USA: National Institue of Standards and Technology, Jul. 2017.

[34] R. C. Langley, "Gold coatings for temperature control in space exploration," *Gold Bull.*, vol. 4, no. 4, pp. 62–66, Dec. 1971.

[35] Y. S. Karavaev, R. M. Kopyatkevich, M. N. Mishina, G. S. Mishin, P. G. Papushev, and P. N. Shaburov, "The dynamic properties of rotation and optical characteristics of space debris at geostationary orbit," *Adv. Astron. Sci.*, vol. 119, pp. 1457–1466, May 2005.

[36] "Helical quadrifilar coilable boom," Orbital ATK, Dulles, VA, USA, Tech. Rep. FS014_15_1, 2005.

[37] C. R. Canizares, "Perspectives on high resolution x-ray spectroscopy," in *Proc. X-Ray Spectrosc. Workshop*, Cambridge, MA, USA: MIT Press, 2007.

[38] "XR-100CR Si-PIN X-ray detector," Amptek, Inc., Dulles, VA, USA, Tech. Rep., 2018.

[39] E. Balsamo *et al.*, "Concept study X-ray testing for NICER's X-ray concentrators," *Proc. SPIE*, vol. 8, p. 8861, Sep. 2013. doi: 10.1117/12.2024108.

[40] T. Okajima *et al.*, "Performance of NICER flight X-ray concentrator," *Proc. SPIE*, vol. 7, Jul. 2016, Art. no. 99054X, doi: 10.1117/12.2234436.

[41] V. Arefiev *et al.*, "Hard x-ray concentrator experiment for Spectrum-X-Gamma mission," *Proc. SPIE*, vol. 6266, Jun. 2006, Art. no. 62663L. doi: 10.1117/12.688428.

[42] H. Schaub and Z. Sternovsky, "Active space debris charging for contactless electrostatic disposal maneuvers," *Adv. Space Res.*, vol. 53, no. 1, pp. 110–118, Jan. 2013.

[43] K. J. H. Phillips, "The solar flare 3.8-10 keV X-ray spectrum," *Astrophys. J.*, vol. 605, no. 2, p. 921, Apr. 2004.

[44] J. R. Winckler, R. Arnoldy, and R. A. Hendrickson, "Echo 2: A study of electron beams injected into the high-latitude ionosphere from a large sounding rocket," *J. Geophys. Res.*, vol. 80, no. 16, pp. 2083–2088, Jun. 1975.

[45] T. Neubert and B. E. Gilchrist, "Relativistic electron beam injection from spacecraft: Performance and applications," *Adv. Space Res.*, vol. 34, no. 11, pp. 2409–2412, 2004.